

Simultaneous source separation using a robust Radon transform

Amr Ibrahim¹ and Mauricio D. Sacchi¹

ABSTRACT

We adopted the robust Radon transform to eliminate erratic incoherent noise that arises in common receiver gathers when simultaneous source data are acquired. The proposed robust Radon transform was posed as an inverse problem using an ℓ_1 misfit that is not sensitive to erratic noise. The latter permitted us to design Radon algorithms that are capable of eliminating incoherent noise in common receiver gathers. We also compared nonrobust and robust Radon transforms that are implemented via a quadratic (ℓ_2) or a sparse (ℓ_1) penalty term in the cost function. The results demonstrated the importance of incorporating a robust misfit functional in the Radon transform to cope with simultaneous source interferences. Synthetic and real data examples proved that the robust Radon transform produces more accurate data estimates than least-squares and sparse Radon transforms.

INTRODUCTION

Several simultaneous source data acquisition methods have been proposed to reduce the cost of seismic surveys and improve illumination by increasing source density (Garotta, 1983; Beasley et al., 1998; Berkhout, 2008; Ikelle, 2010). However, most seismic data processing and imaging techniques are designed to handle data with nonoverlapping sources (conventional acquisition). Therefore, the separation of these blended source data into their equivalent non-overlapped sources data is an important step prior to classical processing sequences. Blending is equivalent to time-shifting data from individual sources and summing them according to a predefined scheme. This blending process can be represented mathematically by the following equation:

$$\mathbf{b} = \Gamma \mathbf{D}, \quad (1)$$

where \mathbf{b} is the blended data, \mathbf{D} represents the original data cube that would be recorded without source overlapping, and Γ is the blending operator. The blending operator can be expressed in the frequency-space domain via the following expression:

$$[\Gamma]_{ij} = e^{i\omega\tau_{ij}}, \quad (2)$$

where τ_{ij} is the delay of the i th source firing time with respect to the detector j and ω indicates the temporal frequency.

Simultaneous source separation (also known as *deblending*) methods can be sorted into two main categories. In the first category, deblending is posed as an inverse problem in which one minimizes a cost function that includes a data misfit and a regularization term. In addition, rather than inverting directly for the deblended data \mathbf{D} , one can invert for the representation of the data in terms of coefficients \mathbf{c} in an auxiliary domain. In other words, if the data are represented in terms of coefficients \mathbf{c} in a basis Φ , such that $\mathbf{D} = \Phi \mathbf{c}$, the aim is to estimate \mathbf{c} by minimizing the following cost function:

$$J = \|\mathbf{b} - \Gamma \Phi \mathbf{c}\|_2^2 + \mu \mathcal{R}(\mathbf{c}). \quad (3)$$

By choosing the appropriate basis Φ , seismic reflections can be focused into a small number of coefficients \mathbf{c} . This is equivalent to synthesizing the data via a sparse collection of basis functions. The regularization term $\mathcal{R}(\mathbf{c})$ is needed because Γ is a noninvertible operator. Algorithms in this category include the sparse Radon inversion (Akerberg et al., 2008; Moore et al., 2008), iterative f - k filtering (Mahdad et al., 2011; Doulgeris et al., 2012), and curvelet-based source separation (Lin and Herrmann, 2009; Wason et al., 2011). This inversion process can also be posed via a projected gradient optimization algorithm (Abma et al., 2010). All these methods attempt to retain coherent signal in common receiver gathers by imposing sparsity in the coefficients \mathbf{c} .

A second category of deblending methods estimates \mathbf{D} directly from the pseudodeblended data:

$$\tilde{\mathbf{D}} = \Gamma^H \mathbf{b} \quad (4)$$

Manuscript received by the Editor 26 April 2013; revised manuscript received 8 October 2013; published online 27 November 2013.
¹University of Alberta, Department of Physics, Edmonton, Alberta, Canada. E-mail: amr.ibrahim@ualberta.ca; msacchi@ualberta.ca.
 © 2013 Society of Exploration Geophysicists. All rights reserved.

via denoising techniques (Beasley et al., 1998; Beasley, 2008; Kim et al., 2009; Huo et al., 2012). Pseudodeblending is equivalent to applying time shifts and dividing long blended records onto the time length of that one would have obtained via standard non-overlapping acquisitions. However, pseudodeblending does not remove interferences resulting from the overlapping of different sources, and pseudodeblended records contain a considerable amount of interferences. Source interferences are coherent in common source gathers and incoherent in common receiver gathers (Berkhout, 2008). The denoising methods use the incoherency of the noise when data are processed in common receiver gathers.

Seismic reflections can be represented by the superposition of hyperbolic events. Consequently, they can be decomposed using hyperbolic Radon transforms. Transformations that use a hyperbolic basis are a variant of the classical Radon transform (Beylkin, 1987). Radon transforms are nonorthogonal transformations, and the accurate recovery of data from the estimated Radon domain is not a simple task. Thorson and Claerbout (1985) suggest treating the problem of estimating the Radon coefficients as an inversion problem. This inversion of the Radon transform demands the inclusion of a regularization term to estimate a stable and unique model. One common approach is the zero-order quadratic (ℓ_2) regularization (Beylkin, 1987). Designing the Radon transform via an ℓ_2 regularization term produces a linear system of equations, and its solution is the estimated Radon coefficients. However, ℓ_2 regularization methods produce unfocused (low-resolution) Radon coefficients (Sacchi and Ulrych, 1995a). Because the Radon basis functions can be tailored to fit the data, one should expect an ideal Radon model that consists of a sparse collection of coefficients. The latter is the idea used by high-resolution (also called sparse) Radon transforms (Thorson and Claerbout, 1985; Sacchi and Ulrych, 1995a, 1995b; Trad et al., 2003). Sparse Radon transforms use a sparsity-promoting regularization term (ℓ_1 or Cauchy norm) and a quadratic misfit function to obtain the data representation in the Radon domain. The quadratic misfit function often results in Radon model coefficients that are sensitive to the presence of erratic noise in the data. This sensitivity can be reduced by adopting a robust misfit function that is capable of modeling data with erratic noise (Claerbout and Muir, 1973). In this case, one can adopt an ℓ_1 misfit function to design Radon transforms that can tolerate erratic noise (Guitton and Symes, 2003; Ji, 2006, 2012; Li et al., 2012).

This article proposes to adopt the robust Radon transform (Ji, 2006, 2012) for deblending seismic data. The robust Radon transform can be incorporated into the deblending problem in two different ways. Similar to the first category of deblending methods, deblended data can be recovered by concatenating the blending and Radon operators and minimizing the cost function given by equation 3 to estimate the vector of coefficients \mathbf{c} that synthesizes the data \mathbf{D} . However, our tests indicate that a more computational efficient approach entails treating the deblending problem via robust Radon transforms as a denoising problem in common receiver gathers (similar to the second category of the deblending methods). In other words, we provide a practical algorithm that uses Radon transforms to denoise common receiver gathers contaminated with erratic noise. The proposed algorithm is used to estimate a noise-free Radon model that synthesizes data free of incoherent interferences.

In our method, the pseudodeblending operator is adopted to separate each blended shot gathers into a data cube composed of common receiver gathers (equation 4). The robust Radon transform using an ℓ_1 misfit is adopted to individually denoise each common receiver gather. We would like to point out that high-resolution (nonrobust) apex-shifted Radon transforms are also proposed by Trad et al. (2012) for fast source separation. Trad et al. (2012) suggest to use the sparse Radon inversion in the common source gather followed by apex domain filtering. They used the difference in location of the reflection hyperbolas apexes for source separation. This is only valid when reflections produced by difference sources have separate apex locations in the Radon model, which is expected in some acquisition schemes.

RADON TRANSFORMS

Transforms that map images and signals into new domains like the Radon transform are a subject of extensive research (Jones, 2013). In general, data are transformed to a new domain to facilitate separation of their components and to differentiate signals from noise. Radon transforms in both frequency and time domains have been used to model seismic reflections and to attenuate the coherent noise. For instance, the parabolic Radon transform (Hampson, 1986) has been widely used for multiple suppression in common midpoint gathers after normal moveout (NMO) correction. Similarly, hyperbolic Radon transforms have been used to attenuate multiples in common midpoint gathers prior to NMO correction. Hyperbolic Radon transforms with shifted apex terms have been proposed to attenuate diffractions (Trad, 2003), to eliminate surface related multiples (Hokstad and Sollie, 2006), to separate a simultaneous source (Trad et al., 2012), and to denoise microseismic data (Sabbione et al., 2013). The improvement of the computational efficiency and accuracy of the Radon transform are subjects of ongoing research. Thorson and Claerbout (1985) are the first authors to cast the Radon transform as an inverse problem. They also propose a sparse inversion method to obtain highly focused Radon gathers in the time domain. The original frequency-domain parabolic Radon transform that Hampson (1986) propose is modified by Sacchi and Ulrych (1995a) to incorporate sparsity as well. Cary (1998) observes that time-domain operators can enforce sparsity in both time and in the Radon parameter simultaneously. Herrmann et al. (2000) propose to redesign Radon operators to deal with aliasing by carrying model weights from nonaliased to aliased frequencies. Robust and high-resolution Radon transforms are explored by Ji (2006, 2012). Recently, Hu et al. (2013) propose to use a fast butterfly algorithm to speed computation of the Radon transform.

In our analysis, we deal with 2D seismic data acquisition, but the same concept can be expanded to the 3D case. We consider the data organized in common receiver gathers that have been obtained via pseudodeblending. To avoid notational clutter, we will designate the common receiver gathers as $d(t, h)$ or in vector form \mathbf{d} . The variables t and h indicate time and offset, respectively. The Radon transform is an integral transform that in its discrete form can be expressed via the following two expressions:

$$\tilde{m}(\tau, \xi) = \sum_h d(t = \tilde{\phi}(\tau, h, \xi), h), \quad (5)$$

$$d(t, h) = \sum_{\xi} m(\tau = \phi(t, h, \xi), \xi), \quad (6)$$

where $\tilde{m}(q, \xi)$ are Radon coefficients that one can obtain using the adjoint Radon operator. The parameter ξ is the Radon parameter that depends on the type of integration path that one adopts for the Radon integral. Popular variants of the Radon transform are the linear, parabolic, hyperbolic, or apex-shifted hyperbolic Radon transform (Table 1). In operator form, the adjoint Radon transform can be expressed as

$$\tilde{\mathbf{m}} = \mathbf{L}^T \mathbf{d}. \quad (7)$$

Similarly, the forward Radon transform can be represented by the following expression:

$$\mathbf{d} = \mathbf{Lm}. \quad (8)$$

We use equation 8 to estimate \mathbf{m} via an inversion procedure. The estimated Radon model is subsequently used to recover an improved version of \mathbf{d} using the forward Radon transform.

ROBUST INVERSION

We assume that the data are contaminated with noise, and therefore we pose the estimation of \mathbf{m} via the minimization of the vector of residuals:

$$\mathbf{r} = \mathbf{d} - \mathbf{Lm}. \quad (9)$$

This is an ill-posed problem, and, therefore, a regularization term must be included to estimate a unique and stable model \mathbf{m} . For example, the ℓ_2 regularization term results in smooth estimates of \mathbf{m} . On the other hand, an ℓ_1 regularization term induces solutions that are sparse. Thus, the inversion problem can be formulated by minimizing the following cost function:

$$J = \|\mathbf{r}\|_p^p + \mu \|\mathbf{m}\|_q^q \\ = \|\mathbf{d} - \mathbf{Lm}\|_p^p + \mu \|\mathbf{m}\|_q^q, \quad (10)$$

where the first term on the right-hand side is the misfit term and the second term is the regularization term. In both terms, we

Table 1. Radon operators: HRT, hyperbolic Radon transform; ASHRT, apex-shifted hyperbolic Radon transform; PRT, parabolic Radon transform; ASPRT, apex-shifted parabolic Radon transform; LRT, linear Radon transform; h , offset; v , velocity; h_0 , apex; q , curvature; and p , dip.

Operator	ξ	$\phi(\tau, h, \xi)$	$\tilde{\phi}(t, h, \xi)$
HRT	$\xi = v$	$t = (\tau^2 + \frac{h^2}{v^2})^{1/2}$	$\tau = (t^2 - \frac{h^2}{v^2})^{1/2}$
ASHRT	$\xi = [v, h_0]$	$t = (\tau^2 + \frac{(h-h_0)^2}{v^2})^{1/2}$	$\tau = (t^2 - \frac{(h-h_0)^2}{v^2})^{1/2}$
PRT	$\xi = q$	$t = \tau + qh^2$	$\tau = t - qh^2$
ASPRT	$\xi = [q, h_0]$	$t = \tau + q(h-h_0)^2$	$\tau = t - q(h-h_0)^2$
LRT	$\xi = p$	$t = \tau + ph$	$\tau = t - ph$

assume that the ℓ_p and ℓ_q norms are given by the general expressions $\ell_p = \sum_i |r_i|^p$ and $\ell_q = \sum_i |m_i|^q$. By minimizing the cost function with respect to the unknown vector of Radon coefficients \mathbf{m} , one finds a solution that honors the observations \mathbf{d} . The parameters p and q represent the exponent of the p -norm of the misfit and the q -norm of the model regularization term, respectively. We adopt $p = 2$ when the data contains Gaussian additive noise. On the other hand, we adopt $p = 1$ when the data are contaminated with erratic (non-Gaussian) noise (Claerbout and Muir, 1973). For the model regularization, we adopt $q = 2$ for low-resolution Radon transforms and $q = 1$ for high-resolution (sparse) Radon transforms.

In this article, we test four Radon transform for the removal of erratic blending noise in common receiver gathers. The first transform is the classical least-squares (nonrobust) Radon transform obtained via quadratic regularization (low resolution) that corresponds to $p = 2$ and $q = 2$ (Hampson, 1986). The second transform is the classical high-resolution (nonrobust) Radon transform (Sacchi and Ulrych, 1995b; Trad et al., 2003) that corresponds to $p = 2$ and $q = 1$. The third transform is the robust Radon transform with quadratic regularization ($p = 1$ and $q = 2$). Finally, the fourth transform is the robust Radon transform with sparse regularization ($p = 1$ and $q = 1$).

Iterative algorithms such as iteratively reweighted least squares (IRLS) can be used to estimate \mathbf{m} when either $p = 1$ or $q = 1$ (Trad et al., 2003). Our implementation of IRLS starts by defining the p (and q) norm by the following expression:

$$\|\mathbf{x}\|_p^p = \sum_i |x_i| |x_i|^{p-2} |x_i| = \|\mathbf{W}_x \mathbf{x}\|_2^2, \quad (11)$$

where $[\mathbf{W}_x]_{ii} = |x_i|^{(p-2)/2}$ and $0 < p \leq 2$. The weighting matrix cannot be computed for $x_i = 0$. Therefore, the weighting matrix for \mathbf{m} will be redefined as follows:

$$[\mathbf{W}_m]_{ii} = \begin{cases} \frac{1}{\sqrt{|m_i|^{2-p}}} & \text{if } m_i > \epsilon_m, \\ \frac{1}{\sqrt{\epsilon_m^{2-p}}} & \text{if } m_i \leq \epsilon_m. \end{cases} \quad (12)$$

Similarly, we redefine the weighting matrix for the residuals as follows:

$$[\mathbf{W}_r]_{ii} = \begin{cases} \frac{1}{\sqrt{|r_i|^{2-q}}} & \text{if } r_i > \epsilon_r, \\ \frac{1}{\sqrt{\epsilon_r^{2-q}}} & \text{if } r_i \leq \epsilon_r. \end{cases} \quad (13)$$

Both ϵ_r and ϵ_m represent small numbers to avoid the singularity at $r = 0$ and $m = 0$. Holland and Welsch (1977) use robust statistics to estimate the optimal value of ϵ_r .

$$\epsilon_r = b_r \frac{\text{MAD}(\mathbf{r})}{0.6745}, \quad (14a)$$

where MAD indicates the median absolute deviation of the residuals \mathbf{r} . The parameter b_r is a tuning parameter. Holland and Welsch (1977) recommend using $b_r = 1.345$. The parameter ϵ_m is computed via the following expression:

$$\epsilon_m = b_m \frac{\max |\mathbf{m}|}{100}, \quad (14b)$$

where b_m is a tuning parameter that in our simulations was selected in an heuristic fashion (Trad et al., 2003; Ji, 2006). We can now represent the inversion by the following new cost function:

$$J = \|\mathbf{W}_r \mathbf{r}\|_2^2 + \mu \|\mathbf{W}_m \mathbf{m}\|_2^2. \quad (15)$$

Thus, we have turned the nonquadratic problem into a sequence of quadratic minimization problems for fixed weighting matrices \mathbf{W}_r and \mathbf{W}_m that depends on unknowns \mathbf{r} and \mathbf{m} , respectively. Equation 15 can be written in its standard form (Hansen, 1998) by a simple change of variable $\mathbf{u} = \mathbf{W}_m \mathbf{m}$:

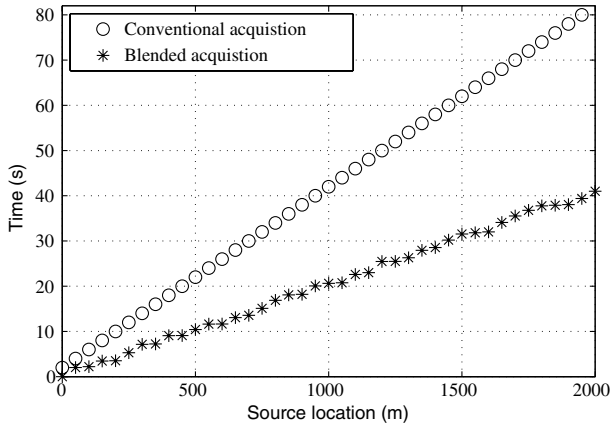


Figure 1. Source firing times for numerically blended synthetic data example.

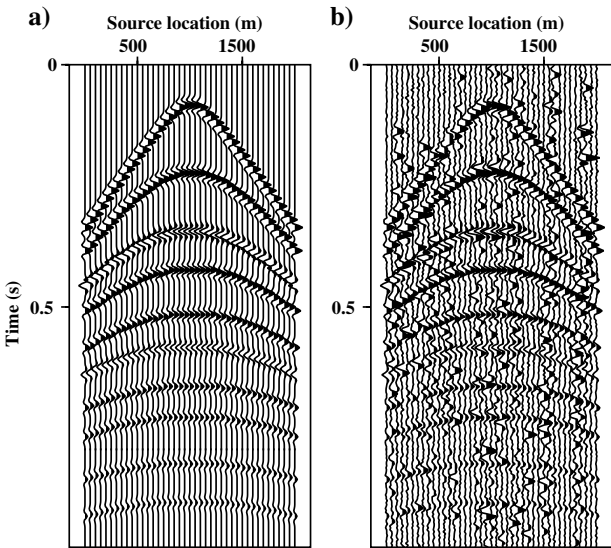


Figure 2. Synthetic data common receiver gather. (a) Original gather. (b) Pseudodeblended gather.

$$J = \|\mathbf{W}_r [\mathbf{L}(\mathbf{W}_m)^{-1} \mathbf{u} - \mathbf{d}]\|_2^2 + \mu \|\mathbf{u}\|_2^2. \quad (16)$$

Equation 16 is minimized via the method of conjugate gradients followed by an update of the matrices of weights \mathbf{W}_r and \mathbf{W}_m . We follow the method described by Trad et al. (2003) in which the regularization term in equation 16 is omitted by setting $\mu = 0$ and the number of iterations of the method of conjugate gradients replaces the trade-off parameter μ (Hansen, 1998). In essence, we have an internal iteration to minimize equation 16 via the method of conjugate gradients and an external iteration to update the weights. The algorithm is stopped when the misfit change between iterations is less than a defined tolerance value (tolerance = 0.01) or when it reaches a maximum number of iterations.

Finally, we want to clarify that the forward Radon operator is also convolved with a wavelet. This permits representing a constant amplitude hyperbola via a single coefficient in the Radon space.

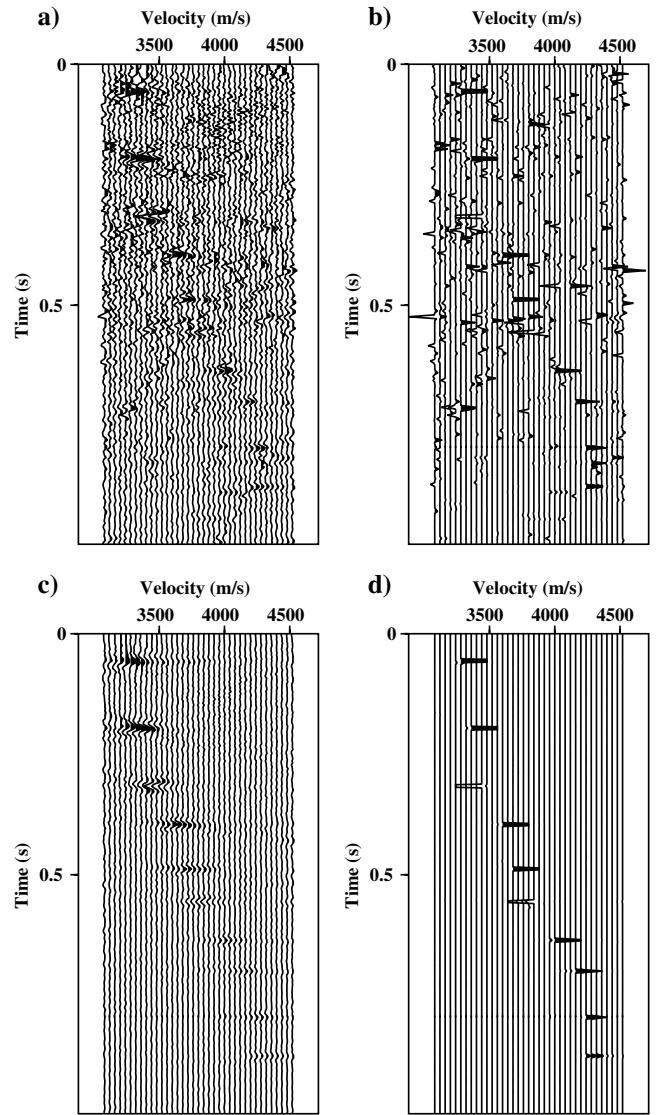


Figure 3. Radon models obtained via inversion with (a) $p = 2$ and $q = 2$, (b) $p = 2$ and $q = 1$, (c) $p = 1$ and $q = 2$, and (d) $p = 1$ and $q = 1$.

Consequently, the adjoint operator requires crosscorrelation with the wavelet. In other words, in our algorithm, we have replaced the operators L by CL and L^T by $L^T C^T$. The operators C and C^T correspond to the convolution and crosscorrelation with a known wavelet, respectively (Claerbout, 1992). We have selected a zero phase wavelet with an amplitude spectrum similar to the amplitude spectrum of the wavelet in the data.

SYNTHETIC EXAMPLE

We tested the robust Radon transform with a blended synthetic data set. The data are numerically blended with a 50% reduction in time compared to conventional acquisition. The firing times of the sources for conventional and blended acquisition sources are shown in Figure 1. The blending scheme represents one-source

firing with random delays. One common receiver gather prior to blending is shown in Figure 2a. The data are numerically blended and pseudoblended into common receiver gathers to obtain Figure 2b.

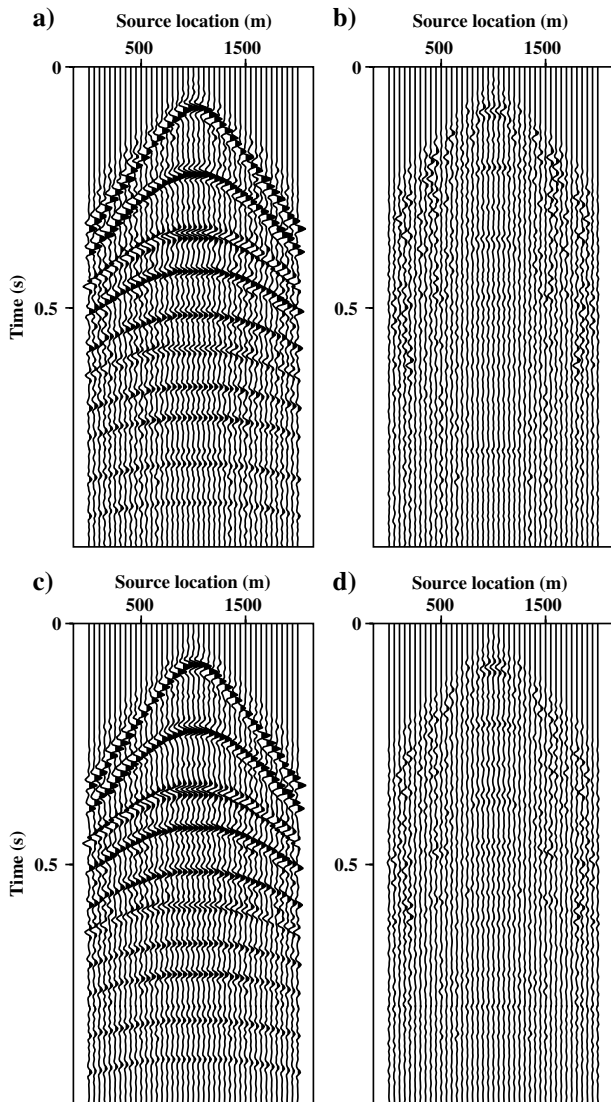


Figure 4. Synthetic common receiver gather recovered using non-robust transforms. (a) Recovered using $p = 2$ and $q = 2$. (b) Error display for (a). (c) Recovered using $p = 2$ and $q = 1$. (d) Error displays for (c).

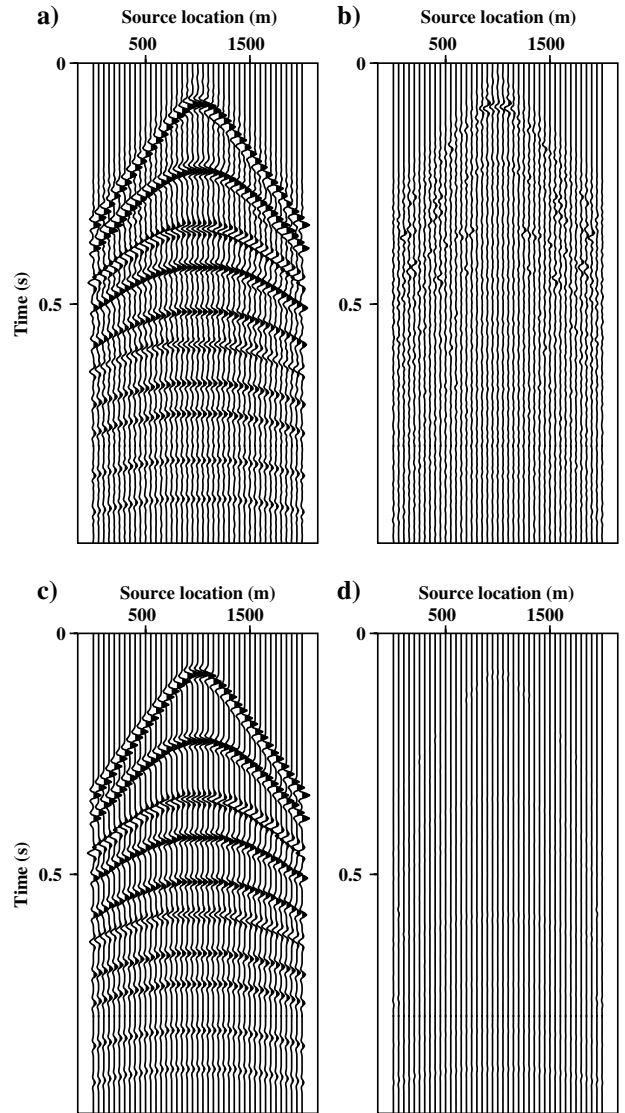


Figure 5. Synthetic common receiver gather recovered using robust transforms. (a) Recovered using $p = 1$ and $q = 2$. (b) Error displays for (a). (c) Recovered using $p = 1$ and $q = 1$. (d) Error display for (c).

Table 2. Q -values of synthetic and real data recovered common receiver gathers.

	$p = 2$ and $q = 2$	$p = 2$ and $q = 1$	$p = 1$ and $q = 2$	$p = 1$ and $q = 1$
Synthetic example	6.38	7.73	10.52	27.56
Real example	7.52	7.63	13.01	12.88

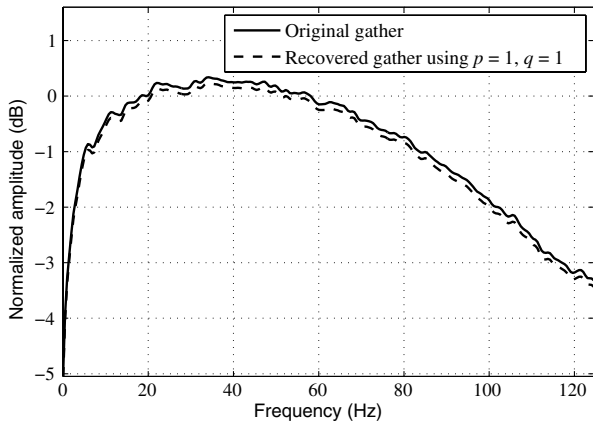


Figure 6. The averaged frequency spectrum of the original and deblended synthetic common receiver gather recovered via the robust Radon transform with $p = 1$ and $q = 1$. The deblended spectrum is shifted slightly downward for clarity.

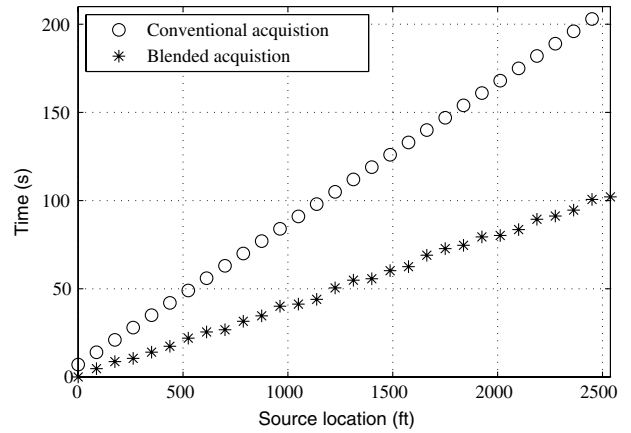


Figure 8. Source firing times for numerically blended real data (only sources number 1–30 are shown for clarity).

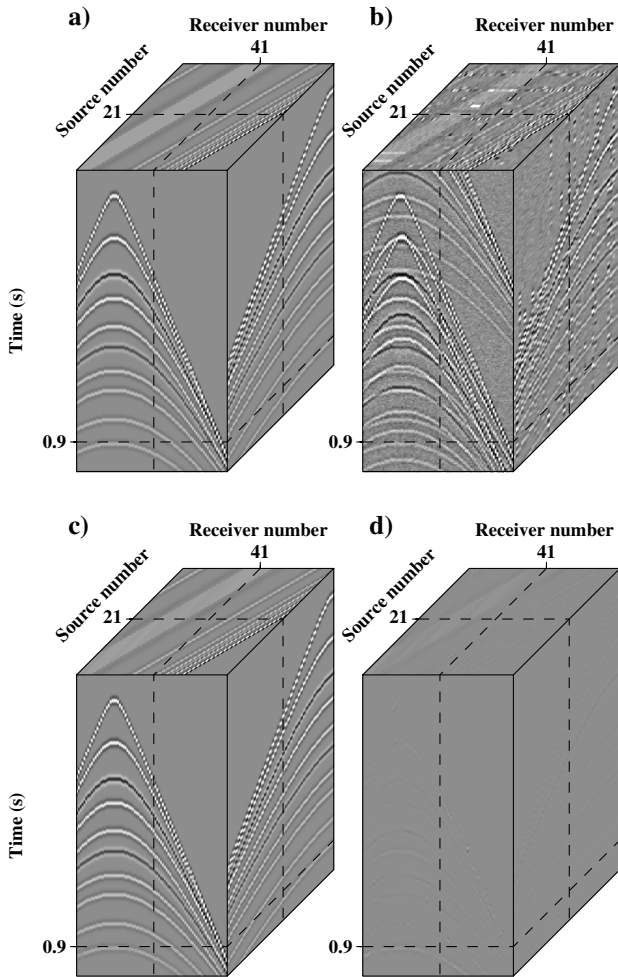


Figure 7. Synthetic data cube. (a) Original data. (b) Pseudodeblended data. (c) Data recovered by forward modeling the Radon coefficients estimated via the robust Radon transform $p = 1$ and $q = 1$. (d) Difference between the recovered and the original data cubes.

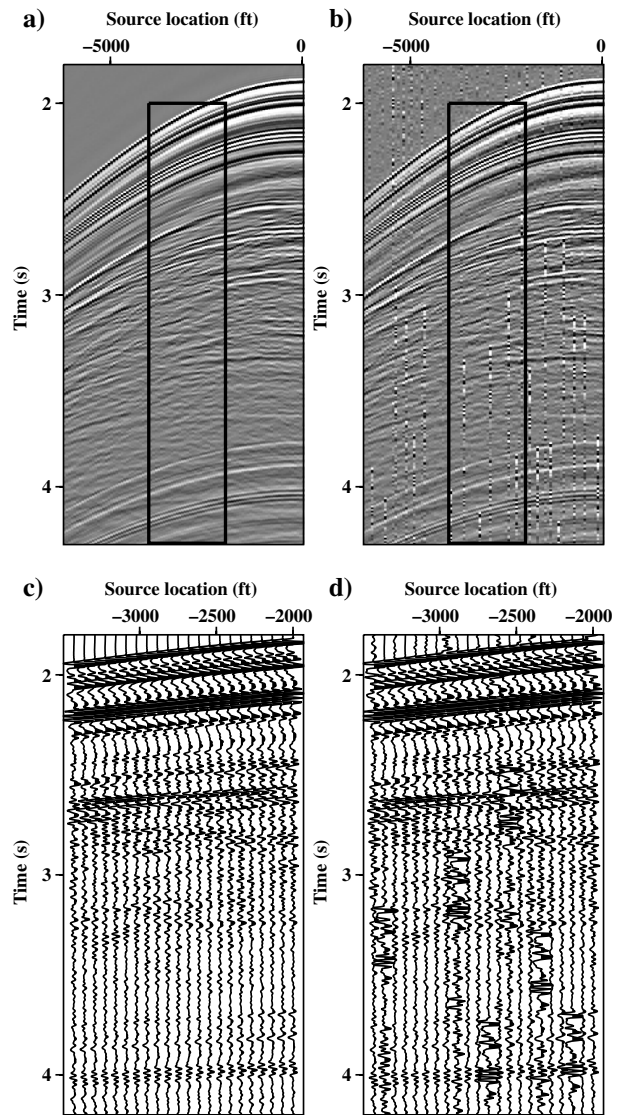


Figure 9. Real data common receiver gather. (a) Original gather. (b) Pseudodeblended gather. (c) Close up of (a). (d) Close up of (b).

The synthetic data are created using a horizontally layered earth model that results in reflection hyperbolas with their apex at zero offset. This permits us to carry out our tests using the hyperbolic Radon transform, which is more computationally efficient than the apex-shifted Radon transform. Radon models estimated from the pseudoblended common receiver gather via the different inversion schemes are shown in Figure 3. The data recovered by forward modeling the nonrobust Radon models are shown in Figure 4a ($p = q = 2$) and 4c ($p = 2, q = 1$). On the other hand, the data recovered from the robust Radon models are shown in Figure 5a ($p = 1, q = 2$) and 5c ($p = 1, q = 1$). The quality of the recovered data is measured using the following expression:

$$Q = 10\text{Log} \frac{\|\mathbf{d}_{\text{original}}\|_2^2}{\|\mathbf{d}_{\text{original}} - \mathbf{d}_{\text{recovered}}\|_2^2}. \quad (17)$$

The Q -values for the recovered synthetic data common receiver gathers are listed in Table 2. The results show that the inversion using both robustness and sparsity ($p = 1, q = 1$) produce the best results (27.56 dB). However, high-quality results were also obtained using the robust Radon transform with quadratic regularization ($p = 1$ and $q = 2$). It is important to stress that the results with the nonrobust Radon transforms were suboptimal for the quadratic and the sparse regularization ($p = 2, q = 1, 2$). Figure 6 shows the average frequency spectrum of the original (noise free) and deblended gather ($p = q = 1$). The average spectrum of the

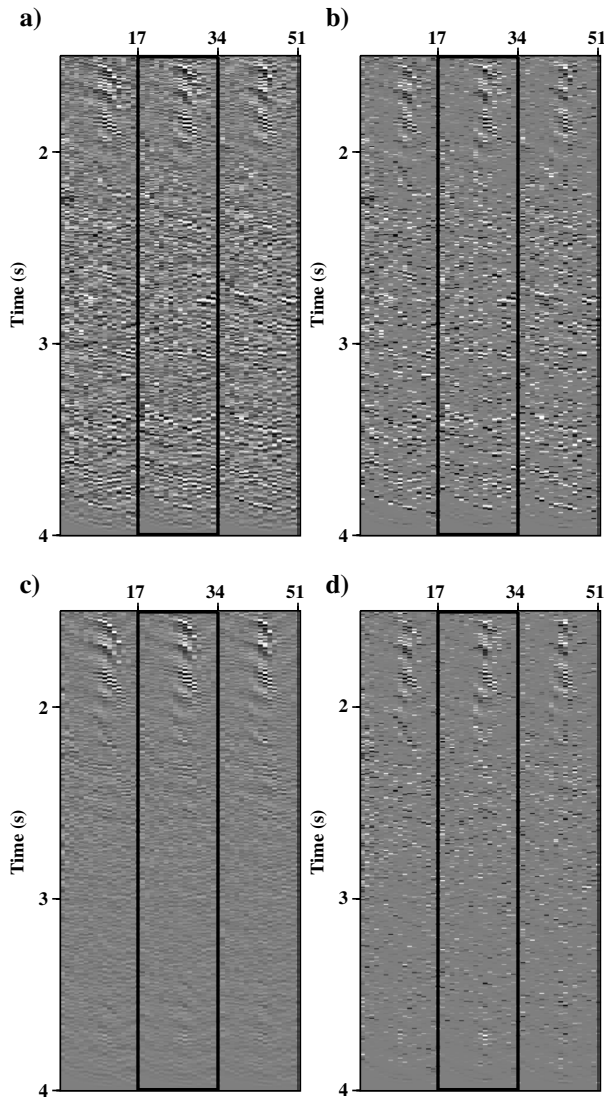


Figure 10. Three velocity panels of the apex-shifted Radon models obtained via inversion with (a) $p = 2$ and $q = 2$, (b) $p = 2$ and $q = 1$, (c) $p = 1$ and $q = 2$, and (d) $p = 1$ and $q = 1$. We show 3 velocity panels of the total of 10 panels used in the apex-shifted Radon transform. The velocity panels correspond to 4400, 4533, and 4666 ft/s. Each velocity panel contains 17 apices ranging from -2800 to 2800 ft.

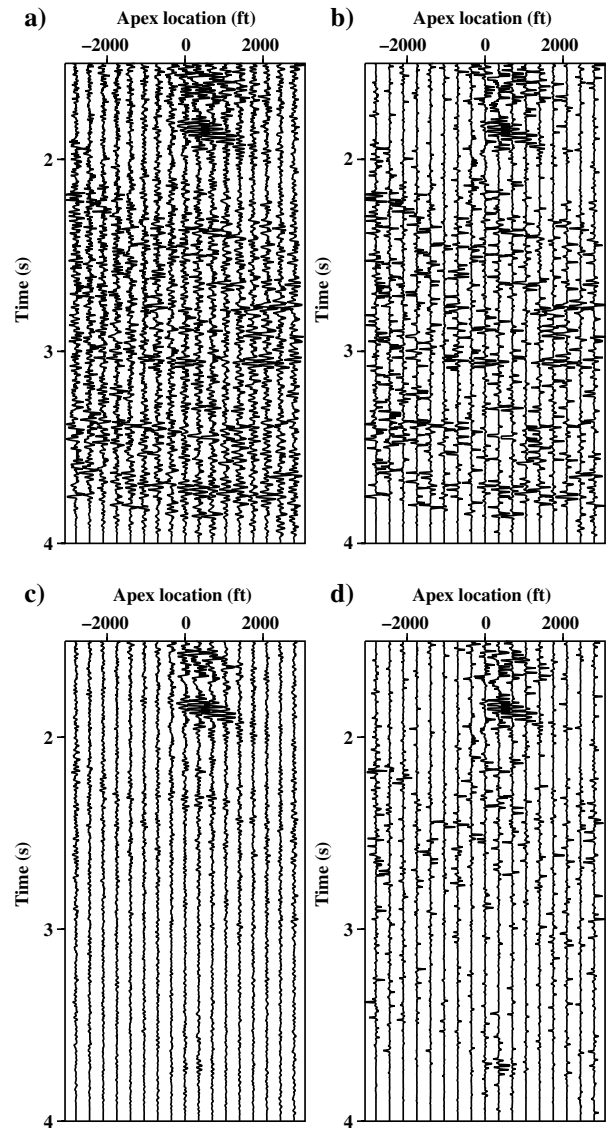


Figure 11. One velocity panel of the apex-shifted Radon models obtained via inversion with (a) $p = 2$ and $q = 2$, (b) $p = 2$ and $q = 1$, (c) $p = 1$ and $q = 2$, and (d) $p = 1$ and $q = 1$. The velocity panel corresponds to 4533 ft/s.

original noise-free common receiver gather is identical to the average spectrum of the deblended gather. Finally, Figure 7 shows the deblended data cube using $(p = 1, q = 1)$ inversion.

REAL DATA EXAMPLE

We also tested the robust Radon transform with a marine data set from the Gulf of Mexico. The data are numerically blended with a 50% time reduction compared to the conventional acquisition. The source firing times versus source location for the first 30 sources (a total of 92 sources are used in this example) are displayed in Figure 8. The blending scheme represents one-source firing with random delays. One common receiver gather prior to blending is shown in Figure 9a, and a close-up of it is shown in Figure 9c.

The data are numerically blended and pseudodeblended into common receiver gathers to obtain Figure 9b, and a close-up of them is shown in Figure 9d.

In this example, we adopt the apex-shifted Radon transform because we cannot guarantee that the reflection hyperbolas apexes are centered at zero offset. The models estimated from the pseudodeblended common receiver gather using different inversion schemes are shown in Figure 10. We found it difficult to impose both sparsity and robustness simultaneously in the case of real data. The sparsity constraint requires representing a single reflection hyperbola with a single Radon coefficient. This is often not feasible with real data due to the mismatch between the theoretical traveltime hyperbola used by the Radon transform and the traveltimes of the actual reflections. Amplitude variations with offset further complicates the problem.

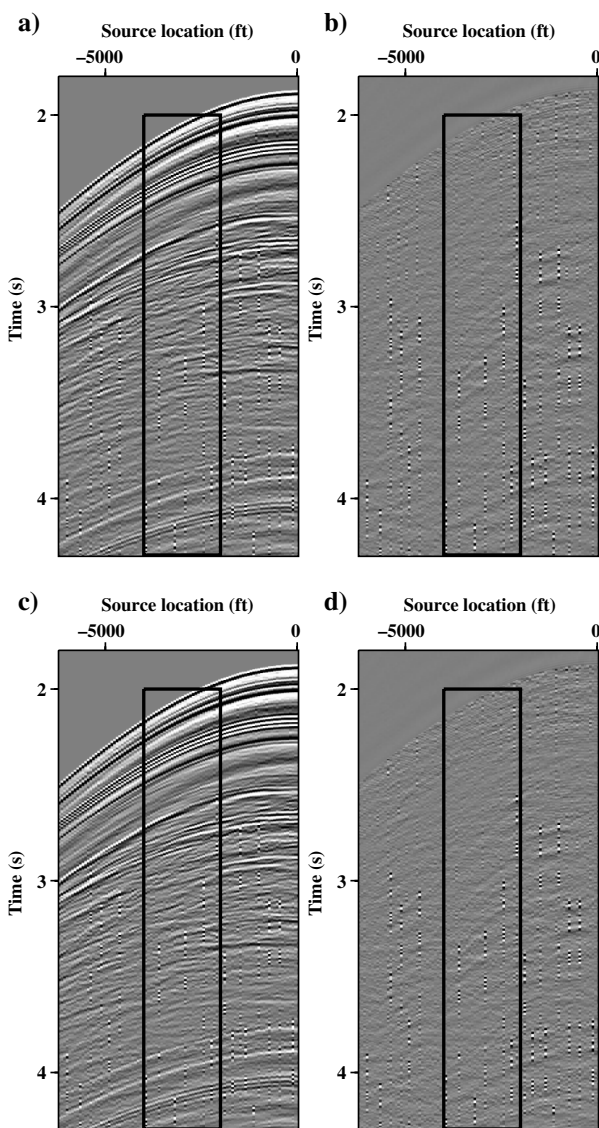


Figure 12. Real data common receiver gather recovered using non-robust inversions. (a) Recovered using $p = 2$ and $q = 2$. (b) Error display for (a). (c) Recovered using $p = 2$ and $q = 1$. (d) Error displays for (c).

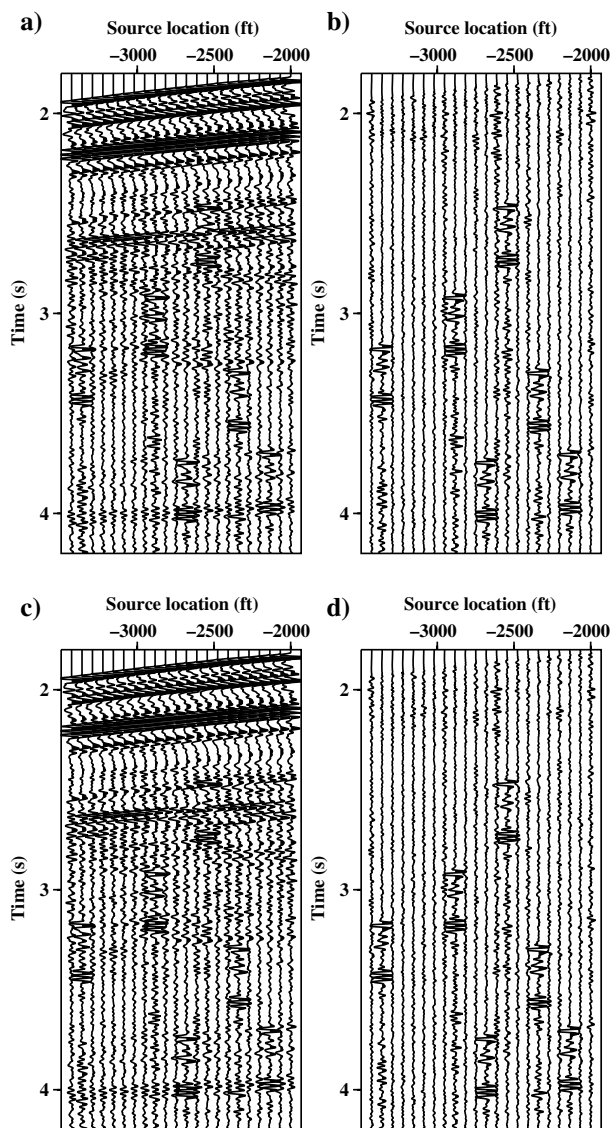


Figure 13. Close-up of real data common receiver gather recovered using non-robust inversions. (a) Recovered using $p = 2$ and $q = 2$. (b) Error display for (a). (c) Recovered using $p = 2$ and $q = 1$. (d) Error displays for (c).

For these reasons, the choice of optimal regularization parameters for robust inversion with sparse regularization ($p = q = 1$) is rather difficult. Five velocity panels (in time, apex), each containing 17 apex locations estimated using different inversion schemes, are displayed in Figure 10. In the Radon transform, we used velocity ranges from 4400 to 5600 ft. The minimum apex corresponds to -2800 ft and the maximum to 2800 ft. We used 10 velocities and 17 apex locations. Notice that only three velocity panels out of 10 are displayed in Figure 10 and only 4533 ft/s velocity panel is shown in Figure 11 for clarity.

The data recovered by forward modeling the nonrobust Radon transforms models are shown in Figure 12a ($p = q = 2$) and 12c ($p = 2, q = 1$). Figure 13 shows a close-up of the nonrobust Radon transforms results that are shown in Figure 12. The data recovered from the robust Radon transforms are shown in Figure 14a ($p = 1,$

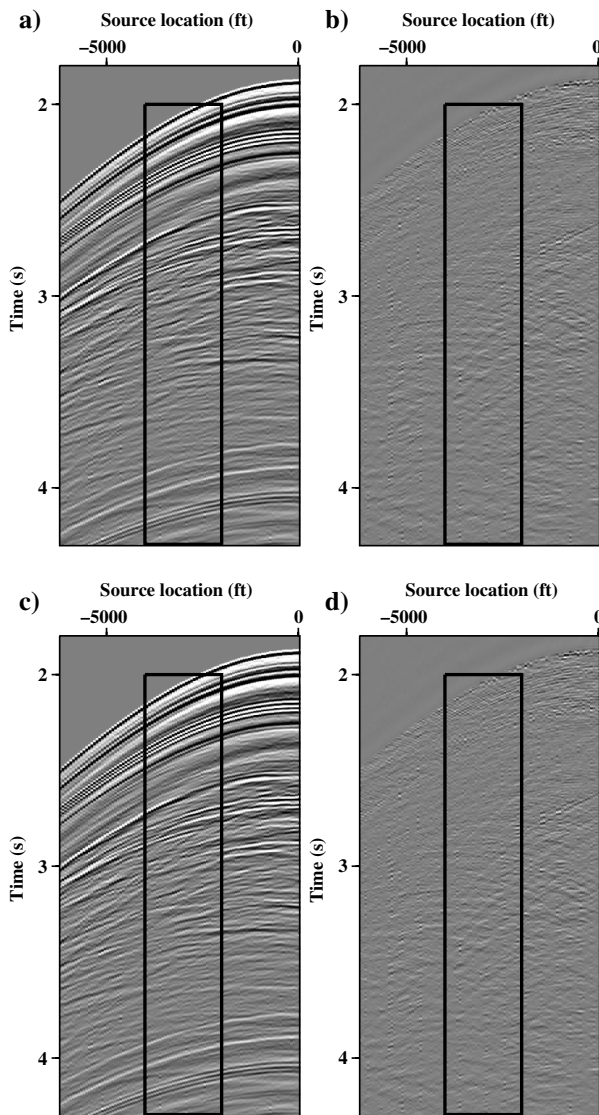


Figure 14. Real data common receiver gather recovered using robust inversions. (a) Recovered using $p = 1$ and $q = 2$. (b) Error display for (a). (c) Recovered using $p = 1$ and $q = 1$. (d) Error displays for (c).

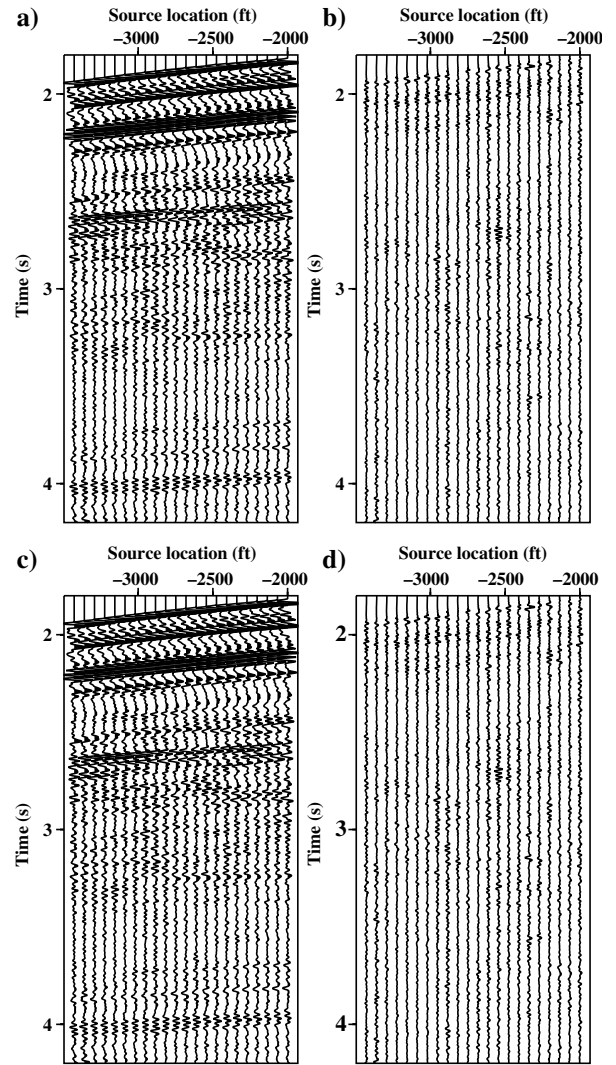


Figure 15. Close-up of real data common receiver gather recovered using robust inversions. (a) Recovered using $p = 1$ and $q = 2$. (b) Error display for (a). (c) Recovered using $p = 1$ and $q = 1$. (d) Error displays for (c).

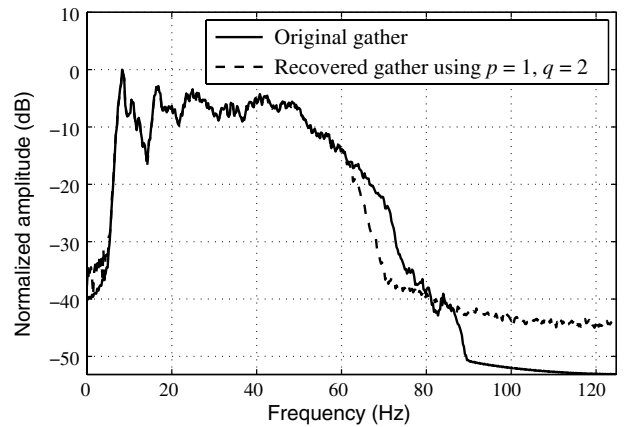


Figure 16. The averaged frequency spectrum of the original and deblended real data common receiver gather recovered via the robust Radon transform with $p = 1$ and $q = 2$.

$q = 2$) and 14c ($p = 1, q = 1$). Figure 15 shows a close-up of the robust Radon transforms results shown in Figure 14. The residuals in Figures 14 and 15 confirm that the robust inversion represents an effective method for removing blending noise. The Q -values for the recovered real data common receiver gathers are listed in Table 2. Our tests show that inversion using both robustness and quadratic regularization ($p = 1, q = 2$) produce the best results ($Q = 13.01$ dB). This illustrates quantitatively that the robust Radon transform can remove the interferences effectively while not degrading the data quality. The frequency spectrum of

the original and the debledned common receiver gather ($p = 1, q = 2$) is shown in Figure 16. The difference between the average spectra in Figure 16 at low and high frequencies could be attributed to additive noise eliminated by our algorithm. Finally, Figure 17 shows the debledned data cube using ($p = 1, q = 2$) inversion.

Regarding the real data example, imposing both robustness and sparsity ($p = q = 1$) is not as simple as one might think. In this case, the algorithm becomes sensitive to the selection of ϵ_r, ϵ_m , and the number of internal and external iterations of the IRLS method. Recent results in the area of robust deconvolution that include sparsity constraints (Gholami and Sacchi, 2012) suggest that more sophisticated algorithms are needed to obtain sparse and robust solutions that are not prone to failure due to incorrect parameter selection (Li et al., 2012).

CONCLUSIONS

We have implemented robust Radon transforms to eliminate the erratic incoherent noise that arises in common receiver gathers when simultaneous source data are acquired. We showed that source interferences in common receiver gathers can be removed via a robust Radon transform.

Our synthetic data example shows superior results when a sparse ($q = 1$) and robust ($p = 1$) Radon transform are adopted. It is well known that the stringent requirement of sparsity can be easily satisfied with simulated data. Conversely, imposing sparsity in the Radon coefficients is not an easy task when there is a mismatch between the traveltimes and amplitudes of the data and those modeled by the transform. The latter limits the benefit of the sparsity constraint for real data applications. However, our real data tests show that the Radon transform with a robust misfit ($p = 1$) and a simple quadratic regularization ($q = 2$) provides an effective algorithm to eliminate erratic source interferences in common receiver gathers.

ACKNOWLEDGMENTS

The authors are grateful to the sponsors of the Signal Analysis and Imaging Group at the University of Alberta. This research was also supported by The Natural Sciences and Engineering Research Council of Canada via a grant to MDS.

REFERENCES

- Abma, R., T. Manning, M. Tanis, J. Yu, and M. Foster, 2010, High quality separation of simultaneous sources by sparse inversion: 72nd Annual International Conference and Exhibition, EAGE, Extended Abstracts, B003.
 Akerberg, P., G. Hampson, J. Rickett, H. Martin, and J. Cole, 2008, Simultaneous source separation by

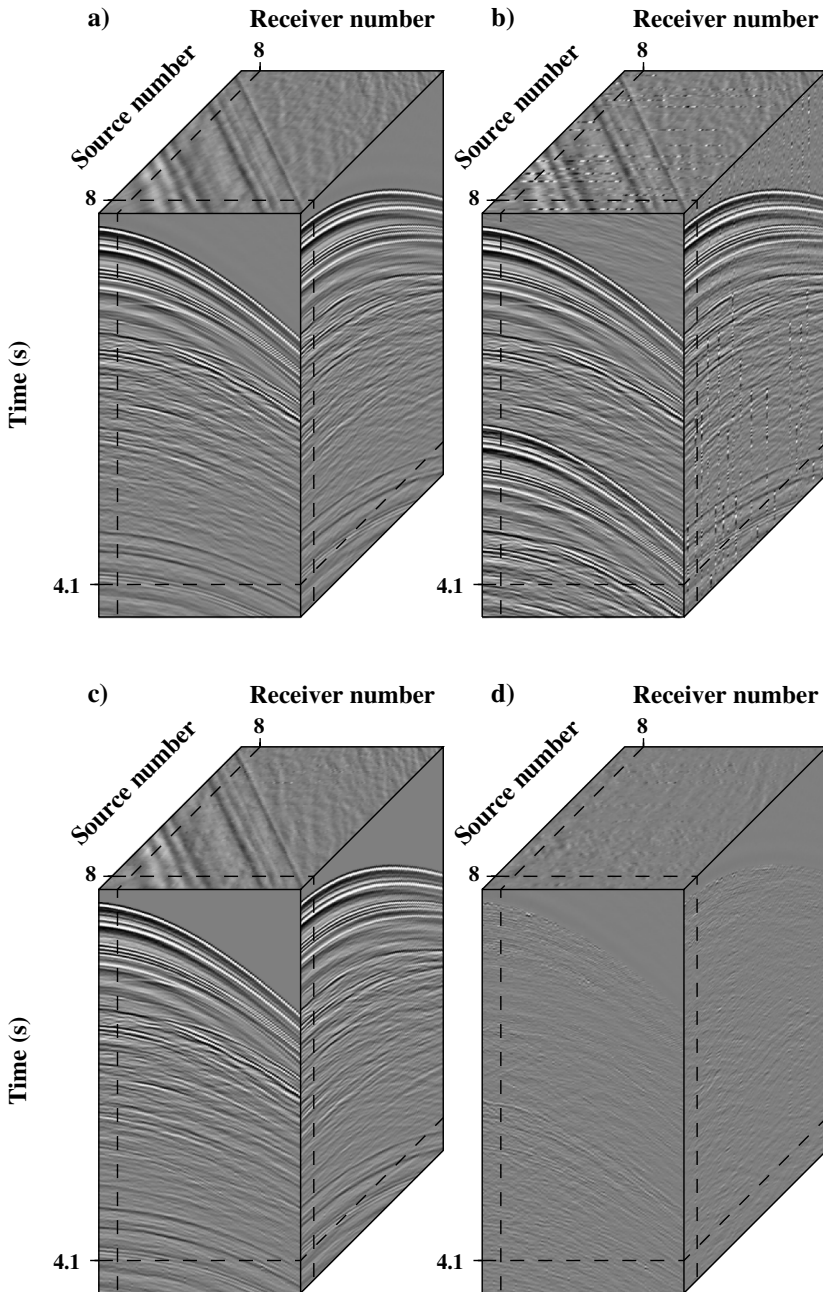


Figure 17. Real data cube: (a) original and (b) pseudodebledned. (c) Data recovered by forward modeling the Radon coefficients estimated via the robust Radon transform $p = 1$ and $q = 2$. (d) Difference between the recovered and the original data cubes.

- sparse Radon transform: 78th Annual International Meeting, SEG, Expanded Abstracts, 2801–2805.
- Beasley, C. J., 2008, A new look at marine simultaneous sources: *The Leading Edge*, **27**, 914–917, doi: [10.1190/1.2954033](https://doi.org/10.1190/1.2954033).
- Beasley, C. J., R. E. Chambers, and Z. Jiang, 1998, A new look at simultaneous sources: 68th Annual International Meeting, SEG, Expanded Abstracts, 133–135.
- Berkhout, A., 2008, Changing the mindset in seismic data acquisition: *The Leading Edge*, **27**, 924–938, doi: [10.1190/1.2954035](https://doi.org/10.1190/1.2954035).
- Beylkin, G., 1987, Discrete Radon transform: *IEEE Transactions on Acoustics, Speech, and Signal Processing*, **35**, 162–172, doi: [10.1109/TASSP.1987.1165108](https://doi.org/10.1109/TASSP.1987.1165108).
- Cary, P. W., 1998, The simplest discrete Radon transform: 68th Annual International Meeting, SEG, Expanded Abstracts, 1999–2002.
- Claerbout, J., 1992, *Earth soundings analysis: Processing versus inversion*: Blackwell Scientific Publications.
- Claerbout, J., and F. Muir, 1973, Robust modeling with erratic data: *Geophysics*, **38**, 826–844, doi: [10.1190/1.1440378](https://doi.org/10.1190/1.1440378).
- Doulgeris, P., K. Bube, G. Hampson, and G. Blacquire, 2012, Convergence analysis of a coherency-constrained inversion for the separation of blended data: *Geophysical Prospecting*, **60**, 769–781, doi: [10.1111/j.1365-2478.2012.01088.x](https://doi.org/10.1111/j.1365-2478.2012.01088.x).
- Garotta, R., 1983, Simultaneous recording of several vibroseis seismic lines: 53rd Annual International Meeting, SEG, Expanded Abstracts, 308–310.
- Gholami, A., and M. D. Sacchi, 2012, A fast and automatic sparse deconvolution in the presence of outliers: *IEEE Transactions on Geoscience and Remote Sensing*, **50**, 4105–4116, doi: [10.1109/TGRS.2012.2189777](https://doi.org/10.1109/TGRS.2012.2189777).
- Guitton, A., and W. W. Symes, 2003, Robust inversion of seismic data using the Huber norm: *Geophysics*, **68**, 1310–1319, doi: [10.1190/1.1598124](https://doi.org/10.1190/1.1598124).
- Hampson, D., 1986, Inverse velocity stacking for multiple elimination: 56th Annual International Meeting, SEG, Expanded Abstracts, 422–424.
- Hansen, P. C., 1998, Rank-deficient and discrete ill-posed problems: Numerical aspects of linear inversion: SIAM, Monographs on Mathematical Modeling and Computation.
- Herrmann, P., T. Mojesky, M. Magesan, and P. Hugonnet, 2000, De-aliased, high-resolution Radon transforms: 70th Annual International Meeting, SEG, Expanded Abstracts, 1953–1956.
- Hokstad, K., and R. Sollie, 2006, 3D surface-related multiple elimination using parabolic sparse inversion: *Geophysics*, **71**, no. 6, V145–V152, doi: [10.1190/1.2345050](https://doi.org/10.1190/1.2345050).
- Holland, P., and R. Welsch, 1977, Robust regression using iteratively re-weighted least-squares: *Communications in Statistics — Theory and Methods*, **6**, 813–827, doi: [10.1080/03610927708827533](https://doi.org/10.1080/03610927708827533).
- Hu, J., S. Fomel, L. Demanet, and L. Ying, 2013, A fast butterfly algorithm for generalized Radon transforms: *Geophysics*, **78**, no. 4, U41–U51, doi: [10.1190/geo2012-0240.1](https://doi.org/10.1190/geo2012-0240.1).
- Huo, S., Y. Luo, and P. G. Kelamis, 2012, Simultaneous sources separation via multidirectional vector-median filtering: *Geophysics*, **77**, no. 4, V123–V131, doi: [10.1190/geo2011-0254.1](https://doi.org/10.1190/geo2011-0254.1).
- Ikelle, L., 2010, *Coding and decoding: Seismic data: The concept of multishooting*: Elsevier Science, Handbook of Geophysical Exploration: Seismic Exploration.
- Ji, J., 2006, CGG method for robust inversion and its application to velocity-stack inversion: *Geophysics*, **71**, no. 4, R59–R67, doi: [10.1190/1.2209547](https://doi.org/10.1190/1.2209547).
- Ji, J., 2012, Robust inversion using biweight norm and its application to seismic inversion: *Exploration Geophysics*, **43**, 70–76, doi: [10.1071/EG12014](https://doi.org/10.1071/EG12014).
- Jones, I. F., 2013, Tutorial: Transforms, orthogonality, eigenvectors, and eigenvalues: *First Break*, **31**, 51–61, doi: [10.3997/1365-2397.2013002](https://doi.org/10.3997/1365-2397.2013002).
- Kim, Y., I. Gruzinov, M. Guo, and S. Sen, 2009, Source separation of simultaneous source OBC data: 79th Annual International Meeting, SEG, Expanded Abstracts, 51–55.
- Li, Y., Y. Zhang, and J. Claerbout, 2012, Hyperbolic estimation of sparse models from erratic data: *Geophysics*, **77**, no. 1, V1–V9, doi: [10.1190/geo2011-0099.1](https://doi.org/10.1190/geo2011-0099.1).
- Lin, T. T., and F. J. Herrmann, 2009, Designing simultaneous acquisitions with compressive sensing: 71st Annual International Conference and Exhibition, EAGE, Extended Abstracts, S006.
- Mahdad, A., P. Doulgeris, and G. Blacquire, 2011, Separation of blended data by iterative estimation and subtraction of blending interference noise: *Geophysics*, **76**, no. 3, Q9–Q17, doi: [10.1190/1.3556597](https://doi.org/10.1190/1.3556597).
- Moore, I., B. Dragoset, T. Ommundsen, D. Wilson, C. Ward, and D. Eke, 2008, Simultaneous source separation using dithered sources: 78th Annual International Meeting, SEG, Expanded Abstracts, 2806–2810.
- Sabbione, J., D. Velis, and M. Sacchi, 2013, Microseismic data denoising via an apex-shifted hyperbolic Radon transform: 83rd Annual International Meeting, SEG, Expanded Abstracts, 2155–2161.
- Sacchi, M., and T. Ulrych, 1995a, High-resolution velocity gathers and offset space reconstruction: *Geophysics*, **60**, 1169–1177, doi: [10.1190/1.1443845](https://doi.org/10.1190/1.1443845).
- Sacchi, M., and T. Ulrych, 1995b, Improving resolution of Radon operators using a model re-weighted least squares procedure: *Journal of Seismic Exploration*, **4**, 315–328.
- Thorson, J. R., and J. F. Claerbout, 1985, Velocity-stack and slant-stack stochastic inversion: *Geophysics*, **50**, 2727–2741, doi: [10.1190/1.1441893](https://doi.org/10.1190/1.1441893).
- Trad, D., 2003, Interpolation and multiple attenuation with migration operators: *Geophysics*, **68**, 2043–2054, doi: [10.1190/1.1635058](https://doi.org/10.1190/1.1635058).
- Trad, D., R. Siliqi, G. Poole, and J. Boelle, 2012, Fast and robust deblending using apex shifted Radon transform: 82nd Annual International Meeting, SEG, Expanded Abstracts, doi: [10.1190/segam2012-0703.1](https://doi.org/10.1190/segam2012-0703.1).
- Trad, D., T. Ulrych, and M. Sacchi, 2003, Latest views of the sparse Radon transform: *Geophysics*, **68**, 386–399, doi: [10.1190/1.1543224](https://doi.org/10.1190/1.1543224).
- Wason, H., F. J. Herrmann, and T. T. Y. Lin, 2011, Sparsity-promoting recovery from simultaneous data: A compressive sensing approach: 81st Annual International Meeting, SEG, Expanded Abstracts, doi: [10.1190/1.3628174](https://doi.org/10.1190/1.3628174).